Adult brains don't fully overcome biases that lead to incorrect performance during cognitive development: an fMRI study in young adults completing a Piaget-like task

Gaëlle Leroux, Jeanne Spiess, Laure Zago, Sandrine Rossi, Amélie Lubin, Marie-Renée Turbelin, Bernard Mazoyer, Nathalie Mazoyer, Olivier Houdé, Marc Joliot

Clinical Neurophysiology 120 (2009) 1501–1513

Contents lists available at ScienceDirect

Clinical Neurophysiology

journal homepage: www.elsevier.com/locate/clinph

Cognitive inhibition of number/length interference in a Piaget-like task: Evidence by combining ERP and MEG ☆

Marc Joliot [a,*], Gaëlle Leroux [a], Stéphanie Dubal [b], Nathalie Tzourio-Mazoyer [a], Olivier Houdé [a,c], Bernard Mazoyer [a,c,d], Laurent Petit [a]

[a] CI-NAPS, Centre d'Imagerie Neurosciences et Applications aux Pathologies, UMR6232, CNRS, CEA, Université de Caen Basse Normandie et Université Paris Descartes, GIP Cyceron, BP 5229, 14074 Caen Cedex, France
[b] UMR 7593, CNRS-UPMC, Centre Emotion, Hôpital de La Salpêtrière, 75651 Paris Cedex 13, France
[c] Institut Universitaire de France (IUF), 103 bd Saint-Michel, 75005 Paris, France
[d] Centre Hospitalier et Universitaire de Caen, 14033 Caen Cedex 9, France

ARTICLE INFO

Article history:
Accepted 4 June 2009
Available online 2 July 2009

Keywords:
Magnetoencephalography
Event-related potential
Inhibition
Late components
Source localizations

ABSTRACT

Objective: We combined event-related potential (ERP) and magnetoencephalography (MEG) acquisition and analysis to investigate the electrophysiological markers of the inhibitory processes involved in the number/length interference in a Piaget-like numerical task.
Methods: Eleven healthy subjects performed four gradually interfering conditions with the heuristic "length equals number" to be inhibited. Low resolution tomography reconstruction was performed on the combined grand averaged electromagnetic data at the early (N1, P1) and late (P2, N2, $P3_{early}$ and $P3_{late}$) latencies. Every condition was analyzed at both scalp and regional brain levels.
Results: The inhibitory processes were visible on the late components of the electromagnetic brain activity. A right P2-related frontal orbital activation reflected the change of strategy in the inhibitory processes. N2-related SMA/cingulate activation revealed the first occurrence of the stimuli processing to be inhibited. Both P3 components revealed the working memory processes operating in a medial temporal complex and the mental imagery processes subtended by the precuneus.
Conclusions: Simultaneous ERP and MEG signal acquisition and analysis allowed to describe the spatio-temporal patterns of neural networks involved in the inhibition of the "length equals number" interference.
Significance: Combining ERP and MEG ensured a sensitivity which could be reached previously only through invasive intracortical recordings.

1. Introduction

Executive functioning includes a series of high-level processes, the main function of which is to facilitate adaptation to new or complex situations. Indeed, even though most of our daily tasks can be performed in a routine way, some situations require the intervention of control mechanisms such as inhibition (resisting interference) and switching (adjusting to change) to produce appropriate performance (Diamond, 2006). Numerous separate functions have been attributed to executive processes, such as inhibition, initiation of behavior, planning an action, judgment and decision making. Here we used an original set of cognitive inhibition tasks adapted from a Piagetian-like numerical task taken from development psychology (Houdé and Guichart, 2001; Houdé and Tzourio-Mazoyer, 2003; Leroux et al., 2006, 2009; Piaget, 1984). Subjects had to resist or not to number/length interference and to switch from one task to another. Resisting number/length interference is a kind of within-task inhibition, while switching is a kind of between-tasks inhibition that is the ability to inhibit the previous task-solving strategy. As a matter of fact, both kinds of inhibitory control are required in many of the simple or complex time-locked daily tasks we have to solve.

As recently mentioned (Collette et al., 2006), one of the crucial challenges of neuroimaging for better characterizing the functional role of brain areas associated with executive functioning, is to take into account not only the localization of cerebral activity but also the temporal pattern of this activity. Using both event-related potentials (ERP) and functional magnetic resonance imaging

☆ Part of the results was presented during the 11th Annual Meeting of the Organization for Human Brain Mapping in Canada, Toronto (2005), part of the ERP data in Leroux et al. (2006).

* Corresponding author. Tel.: +33 (0) 2 31 47 02 07; fax: +33 (0) 2 31 47 02 22.
E-mail address: joliot@cyceron.fr (M. Joliot).

1388-2457/$36.00
doi:10.1016/j.clinph.2009.06.003

(fMRI), we have previously reported a modulation of the amplitude of late electromagnetic components, namely N2 and P3, with the number/length interference (Daurignac et al., 2006; Leroux et al., 2006).

In the present study, we aimed to further investigate the electrophysiological markers of the cognitive inhibition of the number/length interference as function of the level of interference. Accordingly, two conditions with intermediate levels of interference were added to the analysis along with the pure interference and control conditions. Second, while the previous surface analysis demonstrated differences at the scalp level (Daurignac et al., 2006; Leroux et al., 2006), we aimed to get such information at the regional brain level and identify the cortical networks involved in the cognitive inhibition of the number/length interference. Here, we used simultaneous acquisition of ERP and MEG data and maximized the benefits of this multimodal acquisition in terms of detection power and localization bias by using a single source estimation taking in account both signals.

2. Materials and methods

2.1. Subjects

Eleven healthy volunteers (6 men), aged 23 ± 3 years, all right-handed as assessed by the Edinburgh Inventory (Oldfield, 1971), participated in this study. They were free from cerebral abnormality, as assessed by T1-weighted magnetic resonance images of their brains. They had normal vision without correction. All gave their informed written consent to the study, which was accepted by our local ethics committee.

2.2. Tasks

Subjects were presented with two rows of square or rectangular shapes separated by a horizontal line (see Fig. 1). Each row displayed either an equal or a different number of items (one to four shapes), and the subject had to judge their numerical equivalence. They were instructed to respond by pressing a "same-number" button or a "not-the-same-number" button as quickly as possible, without making any errors (the side of the response, using the right or the left hand, was counterbalanced in half of the subjects). When a button was pressed, the computer recorded the subject's reaction time (RT) (measured in milliseconds from stimulus onset) and the stimulus was erased from the screen. Two types of display were set up, called "covariation" (COV) and "interference" (INT). In COV displays, the number of objects and the row length covaried (Fig. 1, left), while in INT displays, the shapes in one of the rows were spread apart, thereby causing number/length interference (Fig. 1, right). This latter display type corresponds to a Piaget-like task (Houdé and Guichart, 2001; see also Piaget, 1984). Since in COV displays the subjects had, by definition, to always respond by pressing the "not-the-same-number" button, while in INT displays they had to press the "same-number" button, it was important to overcome any strategy consisting of a systematic answer. We therefore introduced 20% of displays with "same-number" responses in COV and "not-the-same-number" responses in INT.

2.3. Experimental design

Each subject was tested in one session comprising six runs. The first two runs consisted in a series of COV and INT displays, respectively. The last four runs were pseudo-random series of two displays: INT/COV and COV/INT. The first two runs were composed of 100 stimuli, and the last four of 70 stimuli. The inter-stimulus interval (ISI) was 2700 ± 275 ms. Stimuli were classified according to the stimulus type (COV or INT), and the type of stimulus preceding the considered stimulus (COV or INT) leading to four interference-related conditions: COV after COV (COV_{cov}), COV after INT (COV_{int}), INT after COV (INT_{cov}), or INT after INT (INT_{int}). Such classification creates four classes of stimuli with an increasing level of resistance to the number/length interference from the lowest level (COV_{cov} the control task without interference) to the highest interfering level (INT_{int}). Note that the first 2 runs led to the COV_{cov} and INT_{int} class and the last four runs to the COV_{int} and INT_{cov}.

2.4. Data acquisition

ERP-MEG data were acquired at the MEG center of "La Pitié Salpêtrière" (Paris). A 151-channel whole head magnetoencephalograph (MEG) system (CTF, VSM MedTech, Coquitlam, Canada) was used to simultaneously record the electroencephalographic (64 electrodes), magnetoencephalographic (151 channels) and electrooculographic (4 electrodes) signals.

Scalp voltages were recorded with a cap (EASYCAP, Herrsching-Breitbrunn, Germany) of 64 Ag/AgCl electrodes. A medium or a large cap was chosen depending on the subject's head size. The Cz location was placed on the vertex of the head (10–20 system) and the other midline electrodes on the mid-sagittal plane. The reference electrodes consisted of two linked-earlobe references with a shoulder ground. The electro-oculogram (EOG) was monitored with two right supra-orbital and infra-orbital electrodes (vertical EOG) and two electrodes on the external canthi (horizontal EOG). The electric signals were recorded using CTF amplifiers (64 EEG and two EOG channels, low-pass 100 Hz), and digitized (sampling rate 625 Hz). The scalp voltages between −0.4 s (pre-stimulus) and +1.7 s (post-stimulus) of the onset of each stimulus were recorded.

The magnetic field at 151 positions organized in a helmet shape was recorded using first order radial gradiometers with synthetic 3rd order noise compensation. The sampling rate and pre- and post-stimulus times were similar to those used for the ERP recording.

EEG electrode positions were measured with a Polhemus Fastrack digitizer (Polhemus, Colchester, VT, USA) with reference

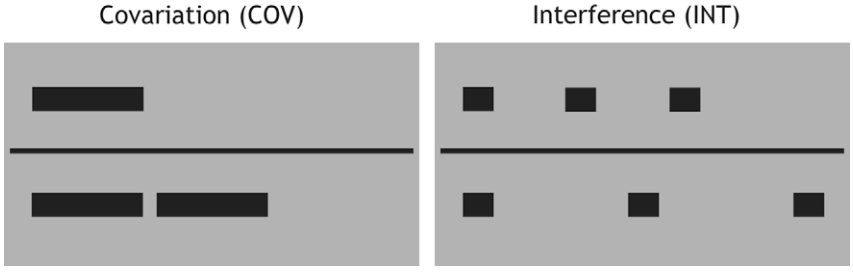

Fig. 1. Experimental design. Subjects must judge the numerical equivalence of two rows displayed on a computer screen. In the "Covariation" item (left) the number and the length co-varied (COV), whereas in the "Interference" item (right) the participants must inhibit (INT) the misleading strategy "length equals number".

to three coils placed on the nasion and near both ears. The location of each MEG detector was automatically measured before and after each run using successive activation of the three coils.

Right after the ERP-MEG, a high-resolution structural T1-weighted sequence MRI (T1-MRI) was acquired at the Caen University Hospital (Signa 1.5T, General Electric, Buc, France) using a spoiled gradient recalled sequence (SPGR-3D, FOV = 240 × 240 × 186 mm^3, sampling = 0.94 × 0.94 × 1.5 mm^3). Radio-opaque markers were positioned at the three reference coil locations of the ERP-MEG session.

At the completion of the ERP-MEG acquisition, the subjects go through a debriefing session where they were asked to describe the strategy used to solve the task.

2.5. Behavioral data processing

Both error rate and response time (RT) were individually computed and subjected to analysis of variance (ANOVA), with conditions (COV_{cov}, COV_{int}, INT_{cov}, INT_{int}) as a within-subject factor.

2.6. Preprocessing of ERP and ERF signals

ERP and MEG data were processed offline using EEGLAB v4.4b (Delorme and Makeig, 2004) and an in-house software.

In the first stage, a two-step artifact-handling procedure was implemented, including a global correction and trial-based manual rejections. For the global correction of eye movement artifacts, we used independent component analysis as described by Jung et al. (2000). This was followed by the automatic detection and suppression of epochs with amplitudes outside the ±100 μV and ±1.5 pT ranges for ERP and MEG, respectively. Additionally, epochs with "improbable values" were suppressed using the procedure implemented in EEGLAB4.4 (Delorme et al., 2004), the threshold being set at five times the standard deviation. On average, the percentage of epochs removed was around 9% (SD = 2%) per subject.

In the second stage, for each subject and each type of signal (ERP and MEG) the average of epochs relevant to each condition (COV_{cov}, COV_{int}, INT_{cov}, and INT_{int}) was computed with a trigger at the onset of visual stimulation. Throughout the paper, MEG averages will be referred as event related field (ERF). Only trials free of artifacts and corresponding to correct answers were included in the individual ERP and ERF averages: 89% (SD = 5%, $N = 11$) of the acquired trials for COV_{cov}, 88% (SD = 3%) for COV_{int}, 90% (SD = 3%) for INT_{cov}, and 91% (SD = 3%) for INT_{int}. Both ERP and ERF averages were band-pass filtered (0.6–30 Hz) with a 200 ms pre-stimulus baseline.

In the last stage, grand averages (ERF and ERP) were computed for each condition (Fig. 2) and across conditions (Fig. 3). While EEG was acquired using a pseudo 10–20 system, the reproducibility of head positioning in the MEG system was only visually checked. To minimize potential discrepancies in the detector locations across subjects, we developed a specific procedure to compute the magnetic data grand average. Detector locations provided by the MEG system were registered with the MRI images of the individual, using the three reference points whose locations were known in both techniques (MEG through coils, MRI through radiographic markers). Each subject's T1-MRI was submitted to stereotaxic normalization (Ashburner and Friston, 1999) on the Montreal Neurological Institute T1-weighted 152 subject average template (T1-MNI template, Collins et al., 1994), and the corresponding non-linear registration matrix was saved to be applied later to each detector location. Using the projection of each detector location in this referential, a helmet grand average was computed. For each detector, grand average ERF data was built as the average of the nearest detector signal in each subject. The same normalization procedure was applied to the ERP data.

2.7. Captor level analysis

Here we describe the classical methodology used in the analysis of the signals related to surface events. This analysis led to a decomposition of the signal in successive time- and polarity-classified components. For each component, the spatial amplitude extrema were submitted to an ANOVA with condition (COV_{cov}, COV_{int}, INT_{cov}, and INT_{int}) as a within-subject factor.

2.7.1. Component identifications

Using the grand average (Figs. 2 and 3), four components were identified using the amplitude extrema of either ERP or ERF data, or both. The components were named according to the ERP nomenclature based on their latencies and polarities: P1, N1, P2, and N2. A fifth P3 component was identified made of two subcomponents (named $P3_{early}$ and $P3_{late}$); their latencies were measured individually on ERF data for each subject and each condition (Leroux et al., 2006).

The amplitudes of the components were individually measured by averaging data between ±10 ms of the component latencies at each detector; both potential and field maps (individual and grand average) were reconstructed using the EEGLAB software. In each map, the local extrema with the relevant polarities were identified.

The P1 component was identified on the ERF signal around 114 ms, and demonstrated in each condition positive-left and negative-right extrema around LT24 and RT24 electrode sites, respectively, corresponding roughly to T7 and T8 in the EEG 10–20 system.

The negative N1 peaked at 155 ms and was minimal in each condition on the ERP signal at two symmetrically posterior sites corresponding to P5 and P6 in the EEG 10–20 system.

The P2 component was identified on both ERP and ERF signals at 195 ms. The ERP maxima were located in each condition at frontal sites F1 and F2. The ERF extrema were symmetrically found at LT34 and RT34, corresponding to TP9 and TP10 in the EEG 10–20 system.

The N2 component local minima were observed on the ERP signal in FCz for the COV_{int}, INT_{cov} and INT_{int} conditions peaking at 290 ms, and were not seen in the COV_{cov} condition due to the masking by the onset of the P3 component.

The P3 component was identified on both ERP and ERF signals as a CPz extrema that became larger in duration and smaller in amplitude from COV_{cov} to COV_{int} to INT_{cov} conditions, and exhibited a double component in the INT_{int} condition (Fig. 2). Individual analysis identified two subcomponents, named $P3_{early}$ and $P3_{late}$; the second was observed in 3, 8, 10, and 11 subjects in the COV_{cov}, COV_{int}, INT_{cov}, and INT_{int} conditions, respectively. These results led us to perform the processing of the $P3_{late}$ only on COV_{int}, INT_{cov}, and INT_{int} conditions.

2.7.2. Effect of the interference level

The amplitudes of each component were submitted to a repeated-measure ANOVA with condition as the within-subject factor. When two symmetrical right/left maxima were uncovered, an electrode factor, called the asymmetry factor, was added and the p-values were adjusted using the Greenhouse–Geisser correction (noted ε). When an ANOVA factor was found significant ($p < 0.05$), post hoc paired t-tests between conditions were reported with an experiment-wise threshold of significance set to $p = 0.05$ Bonferroni corrected.

For both $P3_{early}$ and $P3_{late}$ components, individual analysis enabled additional ANOVA to be performed on the latencies of each P3 sub-component.

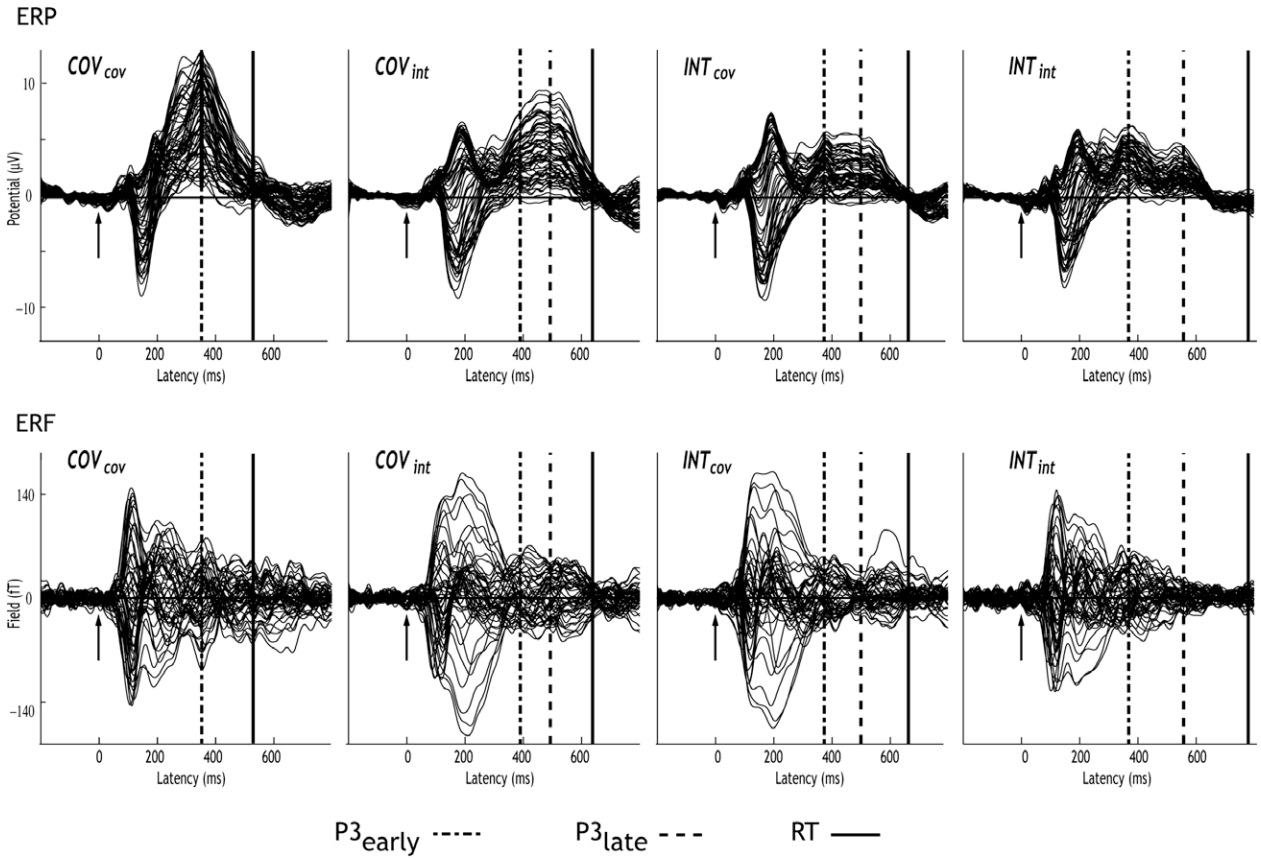

Fig. 2. Butterfly plots of the event-related potentials (ERP) and event-related field (ERF) grand averages for the four conditions: COV_{cov} (COV item after a COV item), COV_{int} (COV item after an INT item), INT_{cov} (INT item after a COV item) and INT_{int} (INT item after an INT item). The thick dashed lines indicate the group $P3_{early}$ and $P3_{late}$ latencies. The thick continuous line indicates response times.

2.8. Combined ERP and ERF source modeling

This analysis was performed in three stages. In the first stage, the CURRY V4.5 software (Neurosoft Inc., Sterling, USA) was used to resolve the inverse problem. In-house developed software was used in the second stage to assess the statistical significance of the similarities and differences between the cortical networks activated in the four interference-related conditions. Finally, the data were submitted to a detailed anatomo-functional descriptive analysis.

2.8.1. Inverse problem

As advocated by others (Yao and Dewald, 2005), among the various algorithms implemented in the CURRY package we chose low resolution tomography (LRT), a minimum norm solution weighted by a Laplacian coupling matrix, initially proposed by Pascual Marqui et al. (1994). Source modeling was computed on the combined ERP and ERF maps of the grand average of each condition (4) and each component (6). Additionally, we computed a solution on 256 noise maps built with the pre-stimulation data. Each of these maps was built by pseudo-randomly selecting chunks of contiguous 20 ms data in each subject, averaging each subject's data (intra-subject), and grand averaging the 11 computed maps (inter-subject). In other words, this procedure was similar to that used to build the map of interest, albeit with pre-stimulus data. Both the grand average detector locations and T1-MNI template were used in the realistic modeling computation. The anatomical volume was used to define in a semi-automatic manner the boundaries of skin, skull, and liquor compartments, which formed the basis of the boundary element model (2026, 2108, and 2572 triangles for skin, skull, and liquor respectively). The source space of the current density estimation was constrained to be inside the liquor shell, and sampled every 4 mm in the three-dimensions. The source modeling at each point of the source space was performed using the LRT with Lp Norm ($p = 1$) and a realistic boundary element forward model. The conductivity factor that defined the relative MEG-to-ERP data weighting (Fuchs et al., 1998) was set at 0.831. It was computed using the first movement-evoked component (MEF1, Joliot et al., 1997), a well-defined tangential source in both MEG and ERP; a specific averaging with a trigger on the response time was computed for this purpose. Note that the computed value was equivalent to the value found by Duzel et al. (2004) using a 35 ms sensorial response to a tactile stimulation. After computation, the 23 component-related and 256 noise-related source models were back-projected in standard T1-MNI template volumes using a tri-linear interpolation to match the initial $2 \times 2 \times 2$ mm^3 resolution.

2.8.2. Statistical analysis

The goal of the second stage was to quantitatively assess, for each latency, the similarities and differences of the neural generators in the four conditions. We first excluded voxels not belonging to the gray matter. This masking was performed on the basis of gray matter segmentation in the T1-MNI template provided with SPM99b (Ashburner and Friston, 1997), with a threshold set at 25%. Each volume was normalized voxel-wise using the average of 256 noise volumes; this process was designed to minimize errors associated with the approximate localization of the detectors. Then, independently for each volume, the cumulative distribution

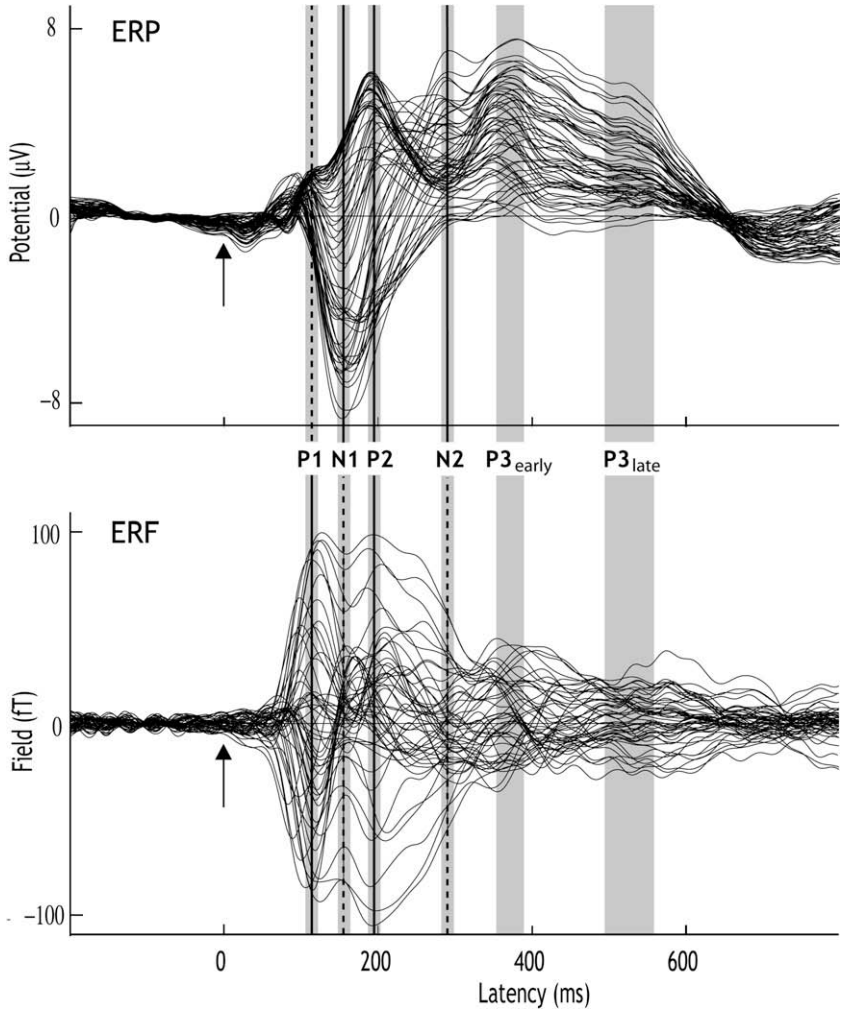

Fig. 3. Butterfly plots of the event-related potentials (ERP) and event-related field (ERF) grand average across four conditions. The latency of each of the first four earliest components is denoted by a shaded line at 114 ± 10 ms for P1, 155 ± 10 ms for N1, 195 ± 10 ms for P2, and 290 ± 10 ms for N2. The continuous or dashed line indicates on which of the ERP or ERF data the component was defined. P1 was defined on both ERF polarity extrema. N1 was defined on the negative ERP data polarities. P2 was defined on the positive ERP data polarities and both ERF data polarities. N2 was defined on the local minima of the ERP data. The shaded thick lines of $P3_{early}$ and $P3_{late}$ indicate the group condition latency ranges deduced from individual data measured on the ERP.

of the voxel values was computed and a rank was affected to each voxel in this distribution between 0 and 1.

For each latency, the network jointly activated in the four interference-related conditions was computed using a voxel-wise conjunction analysis between the N (4, 3 for $P3_{late}$) volumes with a threshold set at $0.95/N$ for each condition. Cortical regions activated in only one condition were also extracted by exclusively masking individual condition volume by the conjunction map and selecting voxels surviving the 0.95 threshold.

2.8.3. Anatomo-functional descriptive analysis

This third stage consisted in describing for each latency cortical regions of high sensitivity and low location bias (Moscher et al., 1993). The selection was performed on the average of 256 noise volumes. The histogram of the latter exhibited a bimodal shape, with the lowest and highest modes segregating the voxels far and near from the detectors, respectively. The minimum between those two modes was selected as the threshold, and a mask was computed including voxels above this threshold. The resulting volumes were rendered in three-dimensions on the SPM99 highly inflated individual brain (Collins et al., 1994) using the Caret 5.3 package (Van Essen et al., 2001). Each volume was decomposed in clusters of at least 150 connected voxels (18 neighborhood node connections); clusters crossing the sagittal median plane were split into two parts. We therefore select the local maxima present in the four interference-related conditions within distances of less than 8 mm. Their mean locations were reported and submitted to the Automated Anatomic Localization software (AAL, Tzourio-Mazoyer et al., 2002). Local maxima amplitude profiles across the four conditions were also presented for selected latencies showing an interference level effect at the captors (see Section 2.7).

Finally, we performed a region of interest (ROI) analysis for the cortical regions activated in only one condition. Such ROIs were defined as the cluster encompassing the local maxima of activation for the considered condition.

3. Results

3.1. Behavioral data

The overall average error rate was <1%. ANOVA revealed a significant overall condition effect ($F[1, 10] = 6.124$, $p = 0.002$) with very low error rate for the first 3 conditions: 0.7%, 0.6%, and 0.2%

for COV_{cov}, COV_{int}, and INT_{cov}, respectively, and 2.4% for INT_{int}. Bonferroni corrected post hoc *t*-test revealed that error rates were significantly higher for INT_{int} than for any of the three other conditions. However, the result was driven toward significance by only two subjects who demonstrated error rates of 5% and 8% in the INT_{int} condition, respectively.

Considering response times (RTs) for the correct answers only, a repeated-measure ANOVA revealed a significant overall condition effect ($F[1, 10] = 30.4$, $p < .0001$) with response time increasing from COV_{cov} (529 ± 117 ms, $N = 11$), COV_{int} (638 ± 59 ms), and INT_{cov} (662 ± 69 ms) to INT_{int} (779 ± 87 ms). All Bonferroni corrected post hoc paired *t*-tests between conditions, with the exception of COV_{int} versus INT_{cov}, were found significant at the 0.05 level.

In the debriefing session subjects reported to use a subitizing strategy based on self-defined assemblies of shapes, and not a shape per row counting strategy.

3.2. Effect of the interference level at the captors

Neither the P1 (ERF and ERP) nor the N1 (ERP and ERF) amplitude ANOVAs revealed a statistically significant interference-related condition effect.

The P2 ERF (but not the P2 ERP) amplitude ANOVA revealed a significant condition effect ($F[3, 30] = 11{,}2$, $p = 0.002$, $\varepsilon = 0.52$) without any asymmetry effect. Post hoc *t*-test demonstrated that both the COV_{cov} and INT_{int} ERF amplitudes were significantly less intense than both COV_{int} and INT_{cov} amplitudes (Fig. 4A).

At the N2 latency, the ERP amplitude ANOVA did not demonstrate any significant effect.

The ANOVA performed on the P3 latencies showed no condition effect, neither on the $P3_{early}$ ($F[3, 30] = 2.6$, $p = 0.07$, mean latency 371 ± 16 ms) nor on the $P3_{late}$ ($F[2, 18] = 2.96$, $p = 0.08$, mean latency 517 ± 35 ms). However, the plot of each latency versus response time (Fig. 4B) confirmed a positive correlation between response times and $P3_{late}$ latency (linear regression slope 0.47), but not with $P3_{early}$ latency (linear regression slope 0.05).

The $P3_{early}$ ERP amplitude ANOVA (measured at the CPz site) showed a significant condition effect ($F[3, 30] = 27.2$, $p < 0.0001$) with a greater COV_{cov} amplitude compared to each other condition and a greater COV_{int} amplitude than INT_{cov} amplitude (Fig. 4C).

For the $P3_{late}$ ERP amplitude, a condition effect was also observed ($F[2, 14] = 17.0$, $p = 0.002$) with a greater COV_{int} amplitude than INT_{cov} or INT_{int} amplitudes (Fig. 4D).

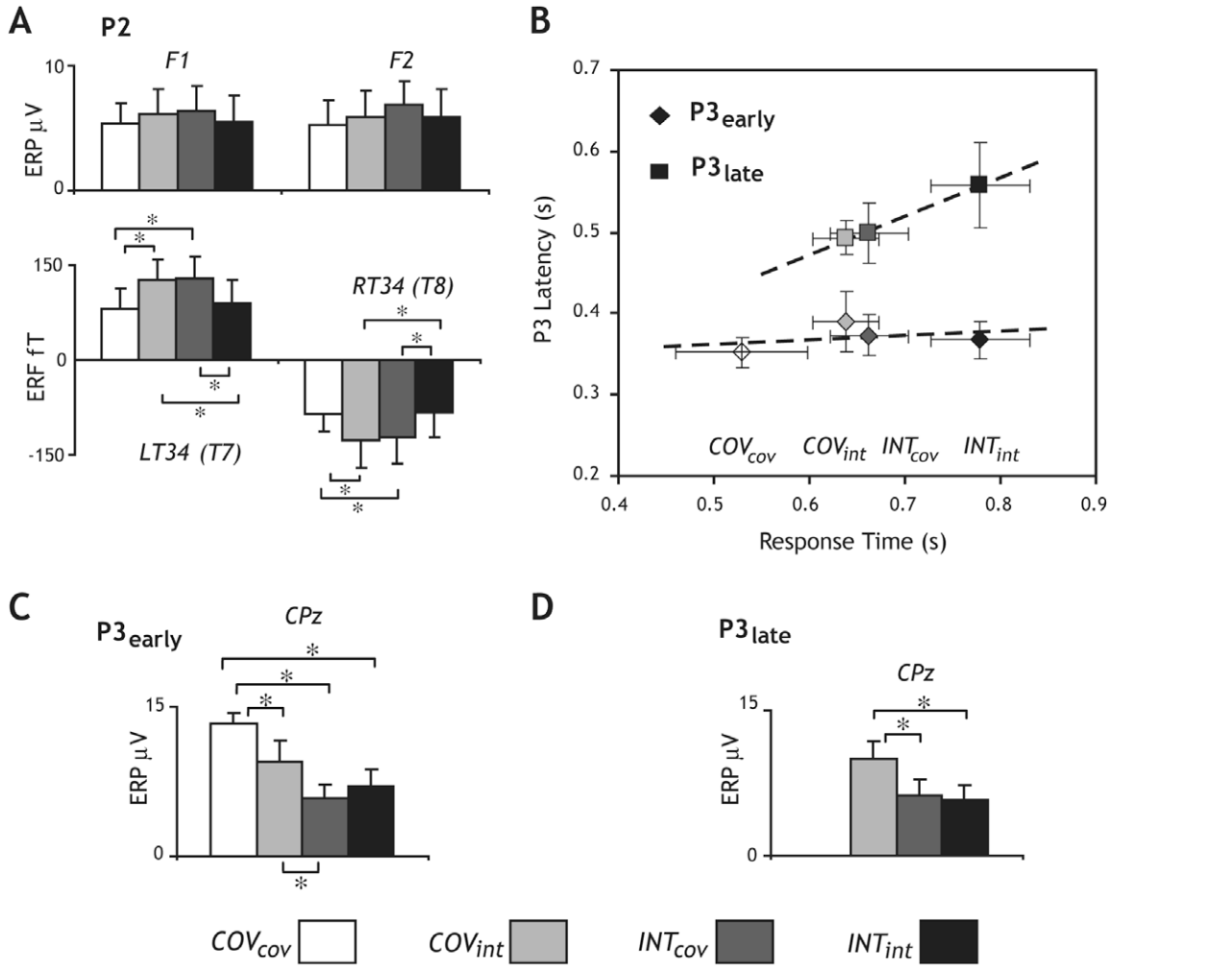

Fig. 4. (A) ERP and ERF P2 amplitude repeated-measure ANOVAs with condition (COV_{cov}, COV_{int}, INT_{cov}, INT_{int}) and asymmetry as within-subject factors. Only the ERF ANOVA on conditions was statistically significant ($p < 0.05$). (B) Plot of $P3_{early}$ and $P3_{late}$ latencies versus response time in each condition. Each value is displayed with ± its standard error at 5%. The linear regression (dashed lines) slope 0.05 and 0.47 slopes are for $P3_{early}$ and $P3_{late}$, respectively. (C) Significant ($p < 0.05$) ERF $P3_{early}$ amplitude repeated-measure ANOVAs with condition as within-subject factor. D) Significant ($p < 0.05$) ERF $P3_{late}$ amplitude repeated-measure ANOVAs with condition as within-subject factor. In panels A, C, and D, the star indicates significant Bonferroni corrected post hoc paired tests ($p < 0.05$) and error bar indicates condition standard error at 5%. The LT24 and RT24 are the MEG denomination of the captor, corresponding roughly to T7 and T8 in the EEG 10–20 system.

3.3. Source modeling

We identified for each latency the cortical network activated by the cognitive inhibition of the number/length interference. In the following, we describe both similarities and differences within this network as function of the level of interference.

3.3.1. Common cortical networks for the four conditions

A conjunction analysis has been performed to extract the activations present in the four interference-related conditions (Table 1, Figs. 5 and 6). For those activations found in the same anatomical location at successive times, the affected latency was chosen as the latency where its volume was maximal.

P1, N1. For the first two latencies, P1 (114 ms) and N1 (155 ms), we observed a set of activations spreading from the occipital cortex toward both the ventral and dorsal visual pathways. This pattern was initiated at 114 ms in the calcarine fissure and bilaterally in extrastriate visual areas, ventrally in the middle/inferior occipital gyri, and dorsally in the superior occipital gyrus up to the superior parietal gyrus and the precuneus. At the 155 ms latency (N1), dorsal activation reached maximum extend in the left angular and superior parietal gyri. In parallel, the ventral activations reached maximum extend bilaterally at the occipito-temporal junctions (Local maxima labeled middle occipital gyrus in the right hemisphere and middle temporal gyrus in the left hemisphere).

P2. For the P2 (195 ms) latency, the largest activation was found in the right frontal orbital region with onset at N1 (Fig. 5, left panel). The corresponding local maxima showed the same amplitude interference-related profile that was depicted by the ERF captor signal analysis that is a higher signal for both COV_{int} and INT_{cov} conditions (Fig. 5, right panel).

We also observed at the P2 latency the peaking in right superior parietal and bilateral medial temporal complex (including the inferior temporal/fusiform gyri, the parahippocampal gyrus, the ventral part the temporal pole). A late reactivation was observed along the left calcarine fissure extending into the posterior part of the lingual gyrus.

N2. For the N2 latency (290 ms), we observed a large activation in the precuneus. The activations localized in the right ventromedial frontal and inferior temporal areas were probably related to the offset of the activations peaking at P2.

$P3_{early}$. For the $P3_{early}$ (371 ms) latency, we observed a set of five regions: the bilateral precuneus, the right medial temporal complex, and both left middle and superior temporal gyri. Different

Table 1
Networks common to the four visuospatial numerical tasks for each of the six components: P1, N1, P2, N2, $P3_{early}$, $P3_{late}$. Cluster anatomical localization, size, and local maxima stereotaxic MNI coordinates (the circled numbers indicate clusters shown in Figs. 5 and 6).

Left			Right		
Local maxima anatomical label	Size (vox.)	x, y, z (mm)	Local maxima anatomical label	Size (vox.)	x, y, z (mm)
P1 (114 ms)					
Calcarine	678	−2, −96, 4			
Middle occipital	868	−23, −95, 7	Middle occipital	572	25, −90, 16
			Inferior occipital	–*	31, −88, −8
Superior occipital	682	−21, −81, 40	Superior occipital	1338	24, −81, 39
Superior parietal	–*	−20, −76, 44	Superior parietal	–*	25, −72, 48
Precuneus	1046	−2, −67, 53	Precuneus	749	3, −65, 53
N1 (155 ms)					
Superior parietal	1055	−21, −74, 44	Superior parietal	383	27, −55, 61
Precuneus	732	0, −65, 51	Precuneus	296	2, −64, 51
Angular gyrus	155	−41, −64, 40			
Middle temporal	1291	−48, −69, 8	Middle occipital	1354	40, −75, 8
Fusiform	1442	−28, 0, −42			
Inferior temporal	–*	−50, −15, −30			
Frontal orbital	866	−24, 36, −20	Frontal orbital	2691	14, 47, −20
P2 (195 ms)					
Calcarine	654	−8, −94, 0			
Lingual	193	−12, −92, −12			
Superior parietal	979	−21, −73, 44	Superior parietal	694	26, −56, 60
Precuneus	912	0, −65, 48	Precuneus	528	2, −65, 48
Middle temporal	917	−48, −67, 9	Middle occipital	1215	40, −74, 12
Inferior temporal	2252	−48, −14, −30	Fusiform	1594	32, 3, −40
Parahippocampal gyrus	–*	−16, −2, −24	Inferior temporal	–*	50, −8, −40
Frontal orbital	1155	−20, 33, −18	Frontal orbital ①	3169	16, 40, −20
N2 (290 ms)					
Superior parietal	170	−12, −68, 44			
Precuneus	1129	0, −64, 48	Precuneus	920	2, −64, 48
			Inferior temporal	889	53, −7, −39
			Frontal orbital	460	9, 39, −13
$P3_{early}$ (371 ms)					
Precuneus ②	857	−1, −65, 52	Precuneus ②	950	2, −64, 52
Middle temporal ③	434	−49, −68, 1			
Superior temporal ④	417	−58, −18, 4			
			Inferior temporal ⑤	2249	33, 1, −42
			Sup. temporal pole	–*	38, 5, −25
			Parahippocampal gyrus	–*	28, 4, −26
$P3_{late}$ (517 ms)					
			Precuneus ②	759	5, −62, 50
Fusiform ⑥	1472	−31, 1, −40	Inferior temporal	940	39, 1, −38
Sup. temporal pole	–*	−31, 6, −28			
Gyrus rectus ⑦	556	0, 49, −20	Gyrus rectus ⑦	314	2, 48, −20

* Localized in the same cluster as above.

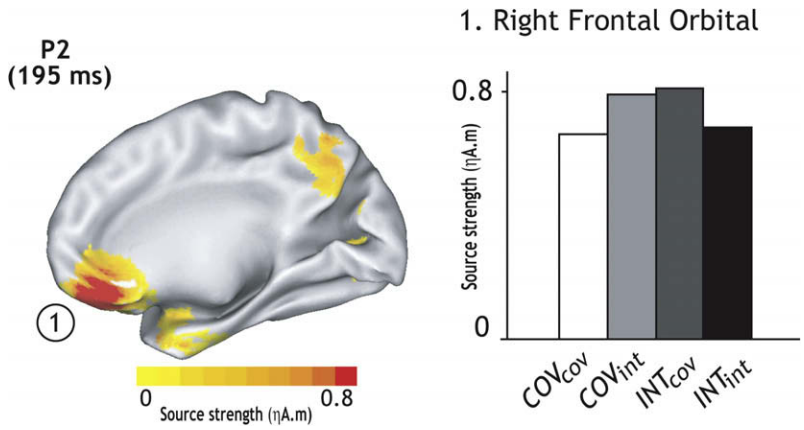

Fig. 5. Left panel: Right Median view of the network common to the four visuospatial numerical tasks at P2 (195 ms). Right panel: Frontal orbital cluster local maxima profile of activation across conditions (number indicates the region listed in Table 1).

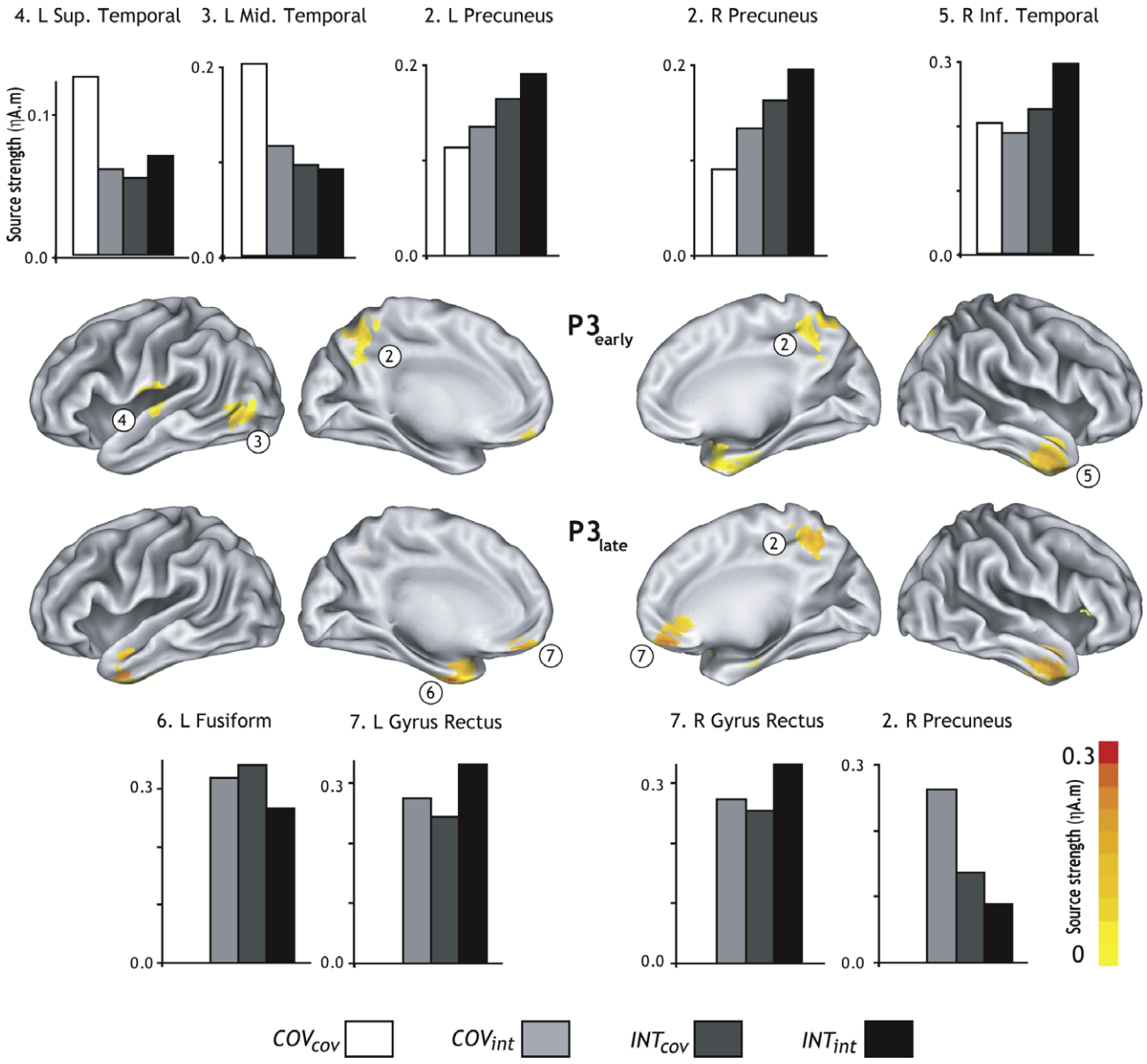

Fig. 6. Upper row: $P3_{early}$ local maxima profile of activation across conditions in the cluster common to the four visuospatial numerical tasks shown on three-dimensional rendering of the cortical surface. Lower rows: Idem for the $P3_{late}$ latency (number indicates the region listed in Table 1).

amplitude patterns were observed for those areas (Fig. 6). The bilateral precuneus activation increased gradually from COV_{cov} to INT_{int} condition. In the INT_{int} condition the right temporal medial complex amplitude was above the amplitude in the three other conditions. On the contrary, both left middle and superior temporal regions showed dominant amplitude in the COV_{cov} condition.

$P3_{late}$. For the $P3_{late}$ (517 ms) latency observed in three conditions only (COV_{int}, INT_{cov}, INT_{int}), we localized activations in the right precuneus and in the left medial temporal complex. A right medial temporal localization was also observed, but is likely to correspond to the offset of the $P3_{early}$ activation of the medial temporal complex. The amplitude pattern of the right precuneus (decreasing from COV_{int} to INT_{int}, Fig. 6) was similar to that observed at CPz on the ERP signal (Fig. 4D).

Finally, small bilateral ventro-medial frontal activations were observed between the gyrus rectus and the orbital part of the superior frontal region.

3.3.2. Regions activated in only one interference-related condition

No cluster reached the extent threshold in a single condition for P1, N1, or P2 latencies.

N2 in the INT_{int} condition. Activation was observed bilaterally in the supplementary motor area/middle cingulate cortex in the INT_{int} condition at the N2 latency (Fig. 7, left panel). The local maxima were located at [0, −14, 60] and [2, −14, 64] on the left and right hemisphere, respectively. ROI analysis computed on the four conditions revealed an increase from COV_{cov} to INT_{int} (Fig. 7, right panel).

$P3_{early}$ in the INT_{cov} condition. A left parahippocampal region was observed at the $P3_{early}$ latency in the INT_{cov} condition, with a local maximum [−27, −3, −31] symmetrical to those observed in its right counterpart in the common network.

$P3_{late}$ in the COV_{int} condition. A left precuneus activation was observed at the $P3_{late}$ latency in the COV_{int} condition, with a local maximum [−1, −62, 46] symmetrical to its right counterparts involved in the common network and mirroring this later, that is with a decreasing amplitude from COV_{int} to INT_{int}.

4. Discussion

Using simultaneous acquisition and source modeling of ERP and MEG signals, we evidenced the electrophysiological markers of the cognitive inhibition of the "length equals number strategy" in a Piaget-like numerical task. To our knowledge, this is the first study to fully describe the temporal pattern of activity within brain networks involved in cognitive inhibition of the number/length processes. The initial activation patterns evoked by every interference-related condition were found in striate and extrastriate visual areas, the superior parietal gyrus and the precuneus about 100–150 ms (P1/N1) after stimulus onset. By 195–290 ms (P2/N2), activation had spread anteriorly to ventral occipitotemporal areas up to the frontal orbital areas. Beyond 370 ms ($P3_{early}$/$P3_{late}$) sustained activation patterns were found in the precuneus, superior and middle temporal gyri and, in a medial temporal complex.

Our goal was also to further investigate the spatiotemporal dynamic of such electrophysiological components as a function of the level of resistance to the number/length interference. The COV_{cov} condition was built to require the lowest level of resistance and other conditions required a gradual increase in cognitive control from the COV_{int} condition to the INT_{int} condition requiring the highest level of resistance. As a matter of fact, behavioral response times showed a gradual increase. The mean error rate in the numerical judgments was very low in every conditions and significantly affected only by the maximum interference level INT_{int} condition which was consistent with our previous study (Daurignac et al., 2006; Leroux et al., 2006).

There are certainly other possible and complementary explanations for the response time difference between COV and INT tasks: for example, INT task, compared with the COV task, might require additional processes such as spatial searching and mental rearranging. Note, however, that these last processes are well part of the executive (i.e. inhibitory) control that we were studying in the Piaget-like task (INT) since this task needs – according to the seminal Piagetian theory (Piaget, 1952, 1984) – the individual's ability to respond to the dimension of number independently of any spatial cues. Executive checking of this independence (i.e. "conservation of number" per se) requires sub-processes such as spatial searching and mental rearranging. Piaget spoke about "operatory reversibility" to describe this procedure for mentally acting on objects: here, to mentally spread apart the objects, then to move them together. Such mental rearranging undoubtedly helps the individuals to inhibit the misleading visuospatial length-equals-number strategy during INT task and contributes also to its cognitive difficulty.

In the following discussion, we will focus on how our combined ERP/MEG approach further enlights the understanding of the spatiotemporal modulation of the cortical network that subtends the cognitive inhibition of the number/length interference.

4.1. Early components and visuospatial processing

The performance of both COV and INT conditions involved the detection of shapes (a set of rectangles), the visuo-spatial exploration of the stimuli, and the onset of the numerical comparison. As a

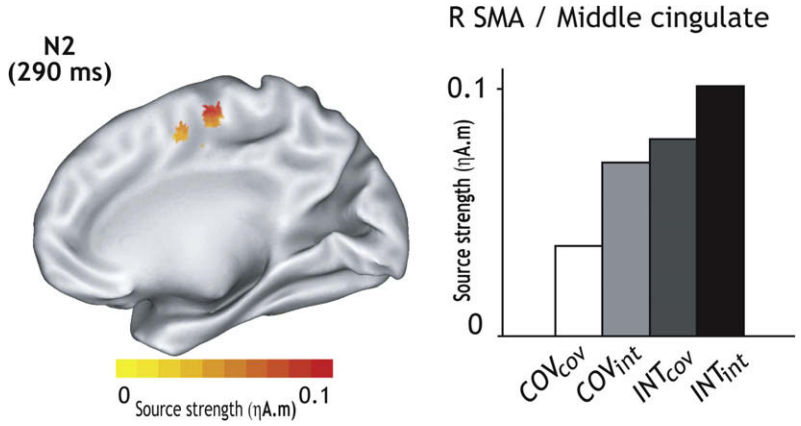

Fig. 7. Left panel: Right Median view of the Supplementary motor area/middle cingulate region significantly activated at N2 in the INT following INT condition (INT_{int}). Right panel: Region of interest profile of activation across conditions.

matter of fact, the set of regions activated at early latencies P1 and N1 encompassed visual and oculomotor areas.

At P1, we observed the peaking of left calcarine and bilateral middle occipital sources, the latter being co-localized with sources of early P1 described by Di Russo et al. (2001) and functionally located in the dorsal V3 retinotopic area (Martinez et al., 2001; Vanni et al., 2004). Bilateral activations were observed along the dorsal stream in the superior occipital and parietal gyri; such activations match the location of the earliest (90–130 ms) saccade-related activation reported by McDowell et al. (2005), also present in our study since the subjects were free to move their eyes to complete the task during all conditions.

Among the regions in which activity peaked at N1, we observed a bilateral occipito-temporal activation, the latency and location of which matched previous findings obtained with combined MEG and cytoarchitectonic or fMRI studies of the MT/V5 area (Barnikol et al., 2006; Vanni et al., 2004; Di Russo et al., 2005). Such activation of the motion-sensitive area could be explained by the rapid and overt shift of attention along the horizontal axis required by evaluation of the stimuli. Alternately, such an area could be part of the dorsal stream (initiated in the inferior occipital at P1) with an activity related to the figurative process used in shape discrimination. Two other regions demonstrated maximal activation at this latency in the left hemisphere: the angular gyrus and the intraparietal sulcus. Both have been described as engaged in numeric processing (Zago and Tzourio-Mazoyer, 2002; Simon et al., 2002; Zago et al., 2008).

Note that no significant difference across interference-related conditions was observed for these early latencies. In other words, the level of number/length interference did not act on the early components during the performance of the current Piaget-like task. This is consistent with our previous findings that showed an effect at later latencies N2 and P3 (Daurignac et al., 2006; Leroux et al., 2006).

4.2. Late components and cognitive inhibition in the number/length processing

Our earlier studies of this Piaget-like numerical task provided a good appraisal of the cognitive inhibition required for its completion (Houdé, 1997; Houdé and Guichart, 2001; Daurignac et al., 2006). Indeed, we previously determined that adult subjects still have to inhibit the "length equals number" heuristic which is an automatic visuospatial bias existing from early childhood, to perform analytical processes and succeed in the numerical task.

Our present results for the late components P2, N2, and P3 shed new light on the cortical network involved in the cognitive inhibition of the number/length interference.

P2. Both ERF surface signals and frontal orbital activation peaking at P2 showed the same dependencies to the interference-related conditions with a highest amplitude for conditions COV_{int} and INT_{cov} that is when a change in the inhibition of the "length equals number" strategy was required. The frontal orbital activation peaking at P2 may therefore stand for the executive control of the toggling between strategies, i.e. for a switching control mechanism. Furthermore, its early onset around N1 indicated a potential top-down process. In their MEG study, Bar et al. (2006) suggested that the left frontal orbital activation may act in a top-down process to facilitate the recognition of objects in the fusiform gyrus through the conveyance of images with low spatial frequency. In the same vein, an ERP study (Potts, 2004) reported bilateral frontal orbital activations similar to ours and hypothesized that frontal orbital areas implement the motivational salience of the stimuli, such regions being at the intersection of the motivational and perceptual systems. Note that in Potts's study the electrode coverage extended unusually low (under the eyes and on the cheeks). We also had extensive brain coverage thanks to the combination of ERP and MEG which, together with the source modeling, allowed to localize the present orbital frontal activation. One may also argue that this result was observed on the ERF signal peaking at P2 while it was probably masked on the ERP signal by the P3 onset.

The other P2-related activations were located bilaterally at the confluence of the anterior fusiform gyrus with the inferior and medial temporal areas, consistent with the MEG study of Bar et al. (2006) who also reported activation in the fusiform gyrus. In the right hemisphere, the earlier onset of the frontal orbital activation relative to the fusiform one that we observed in the right hemisphere was also compatible with the top-down control hypothesis proposed by Bar et al.

N2. Activations related to N2 and common to all the conditions were the continuation of those observed in P2. As a matter of fact, the N2 component shows contributions from both the offset of the P2 and the onset of the P3 because of its temporal situation between both. The set of sources in the superior parietal gyrus, the inferior temporal/fusiform gyri and the right frontal orbital region were clearly related to the offset of the P2 component, while the precuneus activation may be preferentially related to the offset of the P2 and the onset of the $P3_{early}$ components.

We observed a specific activation of the N2 component in the INT_{int} condition which was localized in the supplementary motor area (SMA)/middle cingulate cortex. Using this SMA/cingulate area as a mask, our ROI analysis revealed that its response amplitude increased with the level of interference (Fig. 7). Note that its location appears to be slightly posterior to those described in the conflict monitoring of correct response trials (for a review, see Yeung et al. (2004)). In fact, the localization of the present SMA/cingulate source is prone to be biased toward the close precuneus activation. The mixture of the two source signals made difficult the analysis of the interference-related effect at the scalp surface. The current combined ERP/MEG source modeling allowed a disentanglement of the two activations. We have previously highlighted that the N2 component was the earliest visible trace of the cognitive inhibition (Daurignac et al., 2006; Leroux et al., 2006). Leroux et al. (2006) have notably evidenced an higher amplitude peaking at N2 over the fronto-central area after stimuli with number/length interference (INT) than after number and length covariation (COV). Our combined ERP/MEG approach extends this finding by specifying that the inhibition of the heuristic "number equals length" strategy involves the SMA/cingulate cortex increasingly as the degree of inhibition increased.

P3. This component is usually described as comprising two subcomponents, P3a and P3b, which are associated with involuntary (or novelty) and voluntary detection processes, respectively (Soltani and Knight, 2000). Our paradigm was *a priori* not oriented to create a novelty component. Furthermore, the ERF distribution of activity peaking at $P3_{early}$ and $P3_{late}$ (maximal around CPz) led us to postulate, like others (Gaeta et al., 2003), a P3b-like function for both components. The functional role of the P3b is not firmly established. It is thought to index either the closure of the voluntary stimulus processing or the updating in corticolimbic circuits during attention and working memory (see review in Soltani and Knight (2000)). Most of the source modeling in the P3 component literature has been achieved with data acquired during oddball paradigms with visual, auditory, or somatosensory modality (Polich and Criado, 2006; Soltani and Knight, 2000). Our paradigm was not an oddball task but the models arising about the role of the P3b delineate a general mechanism used in the voluntary processing of stimuli. In the following, we will discuss our results in comparison to the localization results obtained using either single source modeling (ERP or MEG) or intracerebral recording.

The $P3_{early}$ component was reliably extracted in every condition at a constant latency. The classical ERP surface analysis showed

larger $P3_{early}$ amplitude in the control condition (COV_{cov}) as compared to the three interference-related conditions. However, the combined ERP/MEG source modeling allowed us to identify different types of interference-related modulation among the cortical areas peaking at $P3_{early}$.

Common cortical activations evoked at $P3_{early}$ were localized in a right medial temporal complex, in the bilateral precuneus and in the left superior and middle temporal gyri. It constituted a large scale network that possibly fulfilled three cognitive functions: integration of the stimuli, working memory, and mental imagery. The largest $P3_{early}$ activation in the right hemisphere encompassed, the so-called large medial temporal complex, including the inferior temporal/fusiform gyri, the ventral part of the temporal pole, and the parahippocampal region. The localization of this medial temporal complex was consistent with those described by Halgren et al. (reviewed by Halgren et al. (1998)) and others (reviewed by Soltani and Knight, 2000; Brazdil et al., 2003) using intracerebral recording in oddball paradigms. In the context-updating theory, the P3-related medial temporal complex is triggered by working memory processes (Soltani and Knight, 2000). Considering the contribution of the medial temporal lobe in working memory tasks could be unexpected regarding the attribution of medial temporal lobe to the different memory system, i.e. the declarative long-term memory. This traditional distinction between long-term memory processes in the medial temporal lobe and working memory processes in other regions was recently questioned (Ranganath and Blumenfeld, 2005). A series of recent clinical studies in patients with lesions in the medial temporal lobe reported impairments in working memory tasks (e.g. Olson et al., 2006; Nichols et al., 2006; Hannula et al., 2006) and recent neuroimaging studies showed that the median temporal lobe does contribute to working memory (e.g. Ramsoy et al., 2009; Axmacher et al., 2008, 2007).

Stimulus representations maintained in memory from previous exposures, such as in a working memory or recognition task, can produce P3 components to the reoccurrence of that stimulus that are larger than those from stimulus items not previously encountered (e.g., Guo et al., 2006). P3 can also be affected by the rehearsal strategy such that component amplitude was larger for subsequent recall when participants used rehearsal (Fabiani et al., 1990). In other words, the tasks that alter attention devoted to the stimulus and require fundamental memory processing, such as the active maintenance of its representation, affect P3 amplitude. Interestingly, we observed that this right medial temporal complex showed a larger activity in the highest inhibitory demanding task, i.e. INT_{int} condition, when both encoding and rehearsal processes were at most solicited. Note that the present result was directly obtained through the combined ERP/MEG $P3_{early}$ sources that have been unknown by using non-invasive ERP or MEG alone.

We also observed a bilateral activation in the precuneus consistent with the location of activity peaking at $P3_{early}$ in ERP studies of oddball (Crottaz-Herbette and Menon, 2006; Mulert et al., 2004a,b), evaluation of duration (N'Diaye et al., 2004), and working memory tasks (Anurova et al., 2005). According to the review by Cavanna and Trimble (2006), the present activation at $y = -65$ mm in MNI coordinates (corresponding to $y = -60$ mm in Talairach coordinates) was more closely related to the self-centered mental imagery strategy than to episodic memory. This was in accordance with the reported strategy of the subjects that resolved the task using self virtually defined item assemblies, and was confirmed by the observation of a gradual increase in the precuneus activity from COV_{cov}, COV_{int}, and INT_{cov} to INT_{int} conditions.

The last two regions observed in the left hemisphere were located in superior and middle temporal gyri. Both have been previously described in a combined ERP/MEG study concerning spatial auditory memory (Anurova et al., 2005). The superior temporal source has also been described with intracerebral recording as a part of the generator of the P3b. To our knowledge the middle temporal area has not yet been described, and is located in a region that is poorly sampled by intra-cortical recordings (Halgren et al., 1998). Both right temporal regions showed maximal amplitude in the COV_{cov} condition within a modulation pattern similar to that observed at CPz. In addition, the COV_{cov} condition was the only condition in which we did not reliably observe a second P3b component ($P3_{late}$, see below). In agreement with the cognitive model regarding the P3 role (reviewed by Soltani and Knight (2000)), these three observations (localization, modulation, and uniqueness of the P3 component) led us to postulate that these areas may implement the closure of voluntary stimulus processing (Verleger, 1988; Halgren et al., 1998). In fact, the holistic strategy, which took place only when number and length covaried, did not require additional processing (Leroux et al., 2009). It may also reflect the stimuli-to-task significance (Gaeta et al., 2003), high when expectations were fulfilled and smaller when additional processes were required for task completion.

Our results therefore confirmed that the earliest P3b component is indeed a marker of different cognitive processes. Such diversity, which was masked in conventional electrode analysis, was demonstrated by the involvement of cortical areas subtending different cognitive functions. Owing to the fact that some of the described regions have not been previously shown using non-invasive electrophysiological measurements, the benefit of dual ERP/MEG acquisitions/processing gave a definite advantage to decompose the P3 marker into its basic functional components.

Finally, we identified the $P3_{late}$ component in the conditions including number/length interference. The $P3_{late}$ was the only component showing a positive correlation between response times and latencies (Fig. 4B). According to the current models, P3b is not involved in the response selection (see review by Patel and Azzam (2005)). The present $P3_{late}$ dependence upon response times underscored its involvement in the duration of the stimuli evaluation. When turning to the cortical source modeling, we observed a bilateral activation in the precuneus exhibiting decreased amplitude while interference increased. Such a precuneus activity peaking at $P3_{late}$ may be related to the context-closure function, with a specific modulation related to the extraction of lesser information from stimuli (Gaeta et al., 2003) which was the lowest in the condition with the highest interference. Another $P3_{late}$-related activation was located in the left hemisphere at the junction between the left inferior temporal/fusiform gyri and the temporal pole, with no obvious amplitude modulation with the level of number/length interference. As described above for its right counterpart peaking at $P3_{early}$ the current left medial temporal activation may also play a role in the updating triggered by encoding and rehearsal in working memory processes.

The small bilateral activations observed in the gyrus rectus were probably related to the response selection (Roman et al., 2005). Based on the averaging on the response trigger (data not shown) such activation appeared only contralateral to the movement side. The observed bilateral participation was due to the counterbalancing of the hand response in half of the subjects.

4.3. Comparison to our previous fMRI study

Part of the conditions (COV before COV and INT before INT) were also recorded using the fMRI technique (Leroux et al., 2006). While comparison of both techniques was not the primary goal of this paper, such comparison highlights some interesting features. Note however that the fMRI study was based on a block-design paradigm and a region of interest analysis, features which both differed from the current ERP/MEG analysis.

Most of the lateral occipital and parietal areas were found activated with both techniques. It corresponds to the areas observed in the early components of the electromagnetic evoked signal.

Two cases occurred for the regions found activated with the electromagnetic signal analysis and not with the hemodynamic recording. In the first case, we found the frontal orbital activation, peaking at P2, which lies in an area deeply artefacted in the fMRI signal (Ojemann et al., 1997). In fact, only 20% of this area was recorded in fMRI in all the subjects. In the same vein, only 9% of the medial temporal complex was imaged with fMRI. In such a case, the inter-technical comparison could not be fulfilled. The second case concerned the precuneus whose activity was mapped in both fMRI and ERP/MEG. The precuneus was found recurrently activated in the electromagnetic but not in the hemodynamic data. It may be due to the fMRI paradigm that is constructed on the difference image between the considered cognitive process (COV or INT) and a baseline task of lower cognitive charge. This type of analysis elicits in discrete areas deactivations during the target tasks that correspond to activations related to the baseline task (the "default mode" network). This network includes the precuneus (Raichle et al., 2001; Mazoyer et al., 2001; McKiernan et al., 2003) and its activation during the Piagetian task may be overcome by its involvement during the baseline task in the fMRI study.

Activation in the right middle frontal gyrus was detected with fMRI but not with the combined ERP/MEG study. One may argue that in some case of observable fMRI activation the necessary time-locking of activation was not enough to get a component in the electromagnetic signal averaging. We suggested that it was engaged in the mental manipulation necessary for the numerical comparisons (Leroux et al., 2006). Such a process could take place with an important time jitter between the $P3_{early}$ and the $P3_{late}$ latencies which would not allow us to detect it with an ERP/MEG approach.

In conclusion, the present ERP/MEG study provided additional knowledge about the participation of highly integrated areas (precuneus, medial temporal complex) which have been overlooked in the fMRI study.

5. Conclusion

Using simultaneous acquisition and source modeling of ERP and MEG signals, we demonstrated that the inhibitory processes involved when adults performed a Piaget-like numerical task were visible on the late components (P2, N2 and P3) of the electromagnetic brain activity. The right frontal orbital activation peaking at P2 reflected the change of strategy in the cognitive inhibition. The SMA/cingulate activation peaking at N2 revealed the first occurrence of the stimuli processing when the heuristic "number equals length" strategy had to be inhibited. We also observed the multiplicity of cognitive processes taking place at both early and late P3 components. It included both encoding and rehearsal of the working memory processes operating in the medial temporal complex, and the mental imagery processes subtended by the precuneus.

The combined ERP/MEG approach provided a sensitivity which could be reached previously only through invasive intracortical recordings. It was particularly beneficial to reveal the electromagnetic sources located at the vicinity of the boundaries of the recording surfaces. Finally, the combined ERP/MEG source modeling revealed specific condition-dependent modulations that were masked by spatial or temporal proximate sources.

Acknowledgements

We thank Antoine Ducorps of the centre MEG/EEG de la Pitié-Salpêtrière (Paris, France) for his help in data acquisition.

Contract grant sponsors: CEA/Région Basse Normandie, France, and ACI "Neurosciences intégratives et computationnelles" from the French Ministry of Research.

References

Anurova I, Artchakov D, Korvenoja A, Ilmoniemi RJ, Aronen HJ, Carlson S. Cortical generators of slow evoked responses elicited by spatial and nonspatial auditory working memory tasks. Clin Neurophysiol 2005;116(7):1644–54.

Ashburner J, Friston K. Multimodal image coregistration and partitioning-A unified framework. Neuroimage 1997;6:209–17.

Ashburner J, Friston KJ. Nonlinear spatial normalization using basis functions. J Acoust Soc Am 1999;106(1):449–57.

Axmacher N, Mormann F, Fernandez G, Cohen MX, Elger CE, Fell J. Sustained neural activity patterns during working memory in the human medial temporal lobe. J Neurosci 2007;27(29):7807–16.

Axmacher N, Schmitz DP, Weinreich I, Elger CE, Fell J. Interaction of working memory and long-term memory in the medial temporal lobe. Cereb Cortex 2008;18(12):2868–78.

Bar M, Kassam KS, Ghuman AS, Boshyan J, Schmid AM, Dale AM, et al. Top-down facilitation of visual recognition. Proc Natl Acad Sci USA 2006;103(2):449–54.

Barnikol UB, Amunts K, Dammers J, Mohlberg H, Fieseler T, Malikovic A, et al. Pattern reversal visual evoked responses of V1/V2 and V5/MT as revealed by MEG combined with probabilistic cytoarchitectonic maps. Neuroimage 2006;31(1):86–108.

Brazdil M, Roman R, Daniel P, Rektor I. Intracerebral somatosensory event-related potentials: effect of response type (button pressing versus mental counting) on P3-like potentials within the human brain. Clin Neurophysiol 2003;114(8):1489–96.

Cavanna AE, Trimble MR. The precuneus: a review of its functional anatomy and behavioural correlates. Brain 2006;129(Pt 3):564–83.

Collette F, Hogge M, Salmon E, Van der Linden M. Exploration of the neural substrates of executive functioning by functional neuroimaging. Neuroscience 2006;139(1):209–21.

Collins DL, Neelin P, Peters TM, Evans AC. Automatic 3D Intersubject Registration of MR Volumetric Data in Standardized Talairach Space. J Comput Assist Tomograph 1994;18(2):192–205.

Crottaz-Herbette S, Menon V. Where and when the anterior cingulate cortex modulates attentional response: combined fMRI and ERP evidence. J Cogn Neurosci 2006;18(5):766–80.

Daurignac E, Houdé O, Jouvent R. Negative priming in a numerical Piaget-like task as evidenced by ERP. J Cogn Neurosci 2006;18(5):730–6.

Delorme A, Makeig S. EEGLAB: an open source toolbox for analysis of single-trial EEG dynamics including independent component analysis. J Neurosci Methods 2004;134(1):9–21.

Delorme A, Serby H, Makeig S. EEGLAB Tutorial. 2004.

Di Russo F, Martinez A, Sereno MI, Pitzalis S, Hillyard SA. Cortical sources of the early components of the visual evoked potential. Hum Brain Mapp 2001;15(2):95–111.

Di Russo F, Pitzalis S, Spitoni G, Aprile T, Patria F, Spinelli D, et al. Identification of the neural sources of the pattern-reversal VEP. Neuroimage 2005;24(3):874–86.

Diamond A. The early development of executive functions. In: Craik BF, editor. Lifespan cognition: mechanisms of change. New York: Oxford University Press; 2006. p. 70–95.

Duzel E, Habib R, Guderian S, Heinze HJ. Four types of novelty-familiarity responses in associative recognition memory of humans. Eur J Neurosci 2004;19(5):1408–16.

Fabiani M, Karis D, Donchin E. Effects of mnemonic strategy manipulation in a Von Restorff paradigm. Electroencephalogr Clin Neurophysiol 1990;75(2):22–35.

Fuchs M, Wagner M, Wischmann HA, Kohler T, Theissen A, Drenckhahn R, et al. Improving source reconstructions by combining bioelectric and biomagnetic data. Electroencephalogr Clin Neurophysiol 1998;107(2):93–111.

Gaeta H, Friedman D, Hunt G. Stimulus characteristics and task category dissociate the anterior and posterior aspects of the novelty P3. Psychophysiology 2003;40(2):198–208.

Guo C, Duan L, Li W, Paller KA. Distinguishing source memory and item memory: brain potentials at encoding and retrieval. Brain Res 2006;1118(1):142–54.

Halgren E, Marinkovic K, Chauvel P. Generators of the late cognitive potentials in auditory and visual oddball tasks. Electroencephalogr Clin Neurophysiol 1998;106(2):156–64.

Hannula DE, Tranel D, Cohen NJ. The long and the short of it: relational memory impairments in amnesia, even at short lags. J Neurosci 2006;26(32):8352–9.

Houdé O. Numerical development: From the infant to the child. Wynn's (1992) paradigm in 2- and 3-year olds. Cogn Dev 1997;12:373–91.

Houdé O, Guichart E. Negative priming effect after inhibition of number/length interference in a Piaget-like task. Develop Sci 2001;4(1):119–23.

Houdé O, Tzourio-Mazoyer N. Neural foundations of logical and mathematical cognition. Nat Rev Neurosci 2003;4(6):507–14.

Joliot M, Badier JM, Diallo B, Crivello F, Tzourio N, Mazoyer B. PET-MEG spatial correlation in a self-paced motor task. Neuroimage 1997;5(4):S446.

Jung TP, Makeig S, Westerfield M, Townsend J, Courchesne E, Sejnowski TJ. Removal of eye activity artifacts from visual event-related potentials in normal and clinical subjects. Clin Neurophysiol 2000;111(10):1745–58.

Leroux G, Joliot M, Dubal S, Mazoyer B, Tzourio-Mazoyer N, Houde O. Cognitive inhibition of number/length interference in a Piaget-like task in young adults: evidence from ERP and fMRI. Hum Brain Mapp 2006;27(6):498–509.

Leroux G, Spiess J, Zago L, Rossi S, Lubin A, Turbelin M-R, et al. Adult's brain doesn't fully overcome biases that lead to incorrect performance during cognitive development: an fMRI study in young adults completing a Piaget-like task. Dev Sci 2009;12(2):326–38.

Martinez A, DiRusso F, Anllo-Vento L, Sereno MI, Buxton RB, Hillyard SA. Putting spatial attention on the map: timing and localization of stimulus selection processes in striate and extrastriate visual areas. Vision Res 2001;41(10–11):1437–57.

Mazoyer B, Zago L, Mellet E, Bricogne S, Etard O, Houde O, et al. Cortical networks for working memory and executive functions sustain the conscious resting state in man. Brain Res Bull 2001;54(3):287–98.

McDowell JE, Kissler JM, Berg P, Dyckman KA, Gao Y, Rockstroh B, et al. Electroencephalography/magnetoencephalography study of cortical activities preceding prosaccades and antisaccades. Neuroreport 2005;16(7):663–8.

McKiernan KA, Kaufman JN, Kucera-Thompson J, Binder JR. A parametric manipulation of factors affecting task-induced deactivation in functional neuroimaging. J Cogn Neurosci 2003;15(3):394–408.

Moscher JC, Spencer ME, Leahy RM, Lewis PS. Error bounds for EEG and MEG dipole source localization. Electroencephalogr Clin Neurophysiol 1993;86:303–21.

Mulert C, Jager L, Schmitt R, Bussfeld P, Pogarell O, Moller HJ, et al. Integration of fMRI and simultaneous EEG: towards a comprehensive understanding of localization and time-course of brain activity in target detection. Neuroimage 2004a;22(1):83–94.

Mulert C, Pogarell O, Juckel G, Rujescu D, Giegling I, Rupp D, et al. The neural basis of the P300 potential. Focus on the time-course of the underlying cortical generators. Eur Arch Psychiatry Clin Neurosci 2004b;254(3):190–8.

N'Diaye K, Ragot R, Garnero L, Pouthas V. What is common to brain activity evoked by the perception of visual and auditory filled durations? A study with MEG and EEG co-recordings. Brain Res Cogn Brain Res 2004;21(2):250–68.

Nichols EA, Kao YC, Verfaellie M, Gabrieli JD. Working memory and long-term memory for faces: Evidence from fMRI and global amnesia for involvement of the medial temporal lobes. Hippocampus 2006;16(7):604–16.

Ojemann JG, Akbudak E, Snyder AZ, McKinstry RC, Raickle ME, Conturo TE. Anatomical localization and quantitative analysis of gradient refocused echo-planar fMRI susceptibility artifacts. Neuroimage 1997;6:156–67.

Oldfield JC. The assessment and analysis of handedness: the Edimbourgh inventory. Neuropsychologia 1971;9:97–113.

Olson IR, Page K, Moore KS, Chatterjee A, Verfaellie M. Working memory for conjunctions relies on the medial temporal lobe. J Neurosci 2006;26(17):4596–601.

Pascual Marqui RD, Michel CM, Lehmann D. Low resolution electromagnetic tomography: a new method for localizing electrical activity in the brain. Int J Psychophysiol 1994;18(1):49–65.

Patel SH, Azzam PN. Characterization of N200 and P300: selected studies of the event-related potential. Int J Med Sci 2005;2(4):147–54.

Piaget J. The child's conception of number. New York: Basic Books (original in French, 1941); 1952.

Piaget J. Piaget's theory. In: Mussen P. editor. Handbook of child Psychology. New York: Wiley; 1984. p. 103–28.

Polich J, Criado JR. Neuropsychology and neuropharmacology of P3a and P3b. Int J Psychophysiol 2006;60(2):172–85.

Potts GF. An ERP index of task relevance evaluation of visual stimuli. Brain Cogn 2004;56(1):5–13.

Raichle ME, MacLeod AM, Snyder AZ, Powers WJ, Gusnard DA, Shulman GL. A default mode of brain function. Proc Natl Acad Sci USA 2001;98(2):676–82.

Ramsoy TZ, Liptrot MG, Skimminge A, Lund TE, Sidaros K, Christensen MS, et al. Regional activation of the human medial temporal lobe during intentional encoding of objects and positions. Neuroimage 2009.

Ranganath C, Blumenfeld RS. Doubts about double dissociations between short- and long-term memory. Trends Cogn Sci 2005;9(8):374–80.

Roman R, Brazdil M, Jurak P, Rektor I, Kukleta M. Intracerebral P3-like waveforms and the length of the stimulus-response interval in a visual oddball paradigm. Clin Neurophysiol 2005;116(1):160–71.

Simon O, Mangin JF, Cohen L, Le Bihan D, Dehaene S. Topographical layout of hand, eye, calculation, and language-related areas in the human parietal lobe. Neuron 2002;33(3):475–87.

Soltani M, Knight RT. Neural origins of the P300. Crit Rev Neurobiol 2000;14(3–4):199–224.

Tzourio-Mazoyer N, Landeau B, Papathanassiou D, Crivello F, Etard O, Delcroix N, et al. Automated anatomical labelling of activations in spm using a macroscopic anatomical parcellation of the MNI MRI single subject brain. Neuroimage 2002;15:273–89.

Van Essen DC, Dickson J, Harwell J, Hanlon D, Anderson CH, Drury HA. An integrated software system for surface-based analyses of cerebral cortex. J Am Med Inform Assoc 2001;41:1359–78.

Vanni S, Warnking J, Dojat M, Delon-Martin C, Bullier J, Segebarth C. Sequence of pattern onset responses in the human visual areas: an fMRI constrained VEP source analysis. Neuroimage 2004;21(3):801–17.

Verleger R. Event-related potentials and cognition: a critique of the context updating hypothesis and an alternative interpretation of P3. Behav Brain Sci 1988;11:343–56.

Yao J, Dewald JP. Evaluation of different cortical source localization methods using simulated and experimental EEG data. Neuroimage 2005;25(2):369–82.

Yeung N, Cohen JD, Botvinick MM. The neural basis of error detection: conflict monitoring and the error-related negativity. Psychol Rev 2004;111(4):931–59.

Zago L, Petit L, Turbelin MR, Andersson F, Vigneau M, Tzourio-Mazoyer N. How verbal and spatial manipulation networks contribute to calculation: an fMRI study. Neuropsychologia 2008;46(9):2403–14.

Zago L, Tzourio-Mazoyer N. Distinguishing visuospatial working memory and complex mental calculation areas within the parietal lobes. Neurosci Lett 2002;331(1):45–9.